

Journal of Materials Chemistry C

Accepted Manuscript



This is an *Accepted Manuscript*, which has been through the Royal Society of Chemistry peer review process and has been accepted for publication.

Accepted Manuscripts are published online shortly after acceptance, before technical editing, formatting and proof reading. Using this free service, authors can make their results available to the community, in citable form, before we publish the edited article. We will replace this *Accepted Manuscript* with the edited and formatted *Advance Article* as soon as it is available.

You can find more information about *Accepted Manuscripts* in the [Information for Authors](#).

Please note that technical editing may introduce minor changes to the text and/or graphics, which may alter content. The journal's standard [Terms & Conditions](#) and the [Ethical guidelines](#) still apply. In no event shall the Royal Society of Chemistry be held responsible for any errors or omissions in this *Accepted Manuscript* or any consequences arising from the use of any information it contains.

ARTICLE

Supramolecular enhancement of aggregation-induced emission and its application in cancer cell imaging

Cite this: DOI: 10.1039/x0xx00000x

Guocan Yu,^a Guping Tang^b and Feihe Huang^{*a}Received 00th January 2012,
Accepted 00th January 2012

DOI: 10.1039/x0xx00000x

www.rsc.org/

Compared with conventional fluorophores which are often quenched in the aggregate state or at high concentration due to concentration quenching or aggregation caused quenching, tetraphenylethene (TPE)-based organic fluorogens exhibit an extraordinary aggregation-induced emission (AIE) feature, providing a new platform for the development of fluorescence light-up molecules and photostable nanoaggregates for specific analyte detection and imaging. However, self-assembly of TPE-based building blocks can hardly be achieved without introduction of other driving forces due to the propeller-shaped structure and the dynamic rotation of the phenyl rings of the TPE unit. Herein, two four-armed TPE derivatives containing electron-rich naphthalene (TPE-NP) and electron-deficient paraquat (TPE-PQ) groups, respectively, were designed and synthesized. Driven by charge-transfer (CT) interactions, a complex formed between TPE-NP and TPE-PQ. It self-assembled into nanorods in a 1D packing mode, resulting in restriction of intramolecular rotation to enhance the AIE effect significantly. A difunctional negatively charged water-soluble pillar[6]arene (H) was employed to reduce the toxicity and enhance the membrane permeability of TPE-PQ by forming a stable inclusion complex (H₄⊃TPE-PQ) with TPE-PQ. A ternary system containing H, TPE-NP and TPE-PQ was utilized as an imaging agent for cancer cells due to the pH-responsiveness of H. Compared to the physiological pH of 7.4, the pH in tumor tissue and endosomes is more acidic, resulting in the disassembly of the host-guest complex H₄⊃TPE-PQ and the formation of the AIE-enhanced CT complex between TPE-NP and TPE-NP in the cancer cells.

Introduction

Cancer is a leading cause of death worldwide and only modest effects on the survival rate can be achieved by traditional cancer treatment. Accurate identification of cancer cells vs normal cells plays a significant role in the clinical diagnoses and prognoses of various types of cancers. The interstitial pH in malignant tumors is lower than that in normal tissues as a result of increased lactic acid production and reduced buffering and perfusion, which can be employed to selectively detect cancer cells. Fluorescence imaging has been one of the most powerful techniques for the detection of cancer cells without altering regular cellular functions due to its high specificity and sensitivity.¹ Various sophisticated fluorescence probes, such as fluorescent proteins, organic dyes, upconversion nanophosphors, semiconductor nanocrystals, and other nanoparticles, have been designed for this purpose.² Typically, light emissions from conventional fluorophores are quenched in the aggregate state or at high concentration due to aggregation caused quenching (ACQ), which greatly limits the labeling degree of fluorophores to cancer cells, resulting in significant compromise of sensitivity and posing a formidable hurdle to detect cancer cells.³ In contrast to the ACQ effect, Tang *et al* have developed a novel class of organic luminogens, such as tetraphenylethene

(TPE), with extraordinary aggregation-induced emission (AIE) features, which are non-emissive in solution but are induced to luminesce intensely in the aggregate state through restriction of intramolecular rotation (RIR) of the benzene rings of the TPE unit.^{4,5} A series of AIE-based fluorescent probes have emerged for the detection of a wide range of biomolecules in the past decade, because the AIE-active fluorogens exhibit unique fluorescence turn-on properties with high sensitivity and contrast. Various methods, including covalent and noncovalent modification of TPE derivatives, have been employed to restrict the intramolecular rotation of the aromatic rings to achieve the AIE effect. Among them, supramolecular approaches to modify the AIE-active fluorogens are especially important for biocompatibilization and bioapplications, because the unique properties of the fluorogens can be effectively preserved.⁶ Noncovalent interactions,⁷ such as hydrogen bonding, hydrophobic interactions, π - π stacking interactions, electrostatic interactions, and charge-transfer interactions have been employed as driving forces to restrict the intramolecular rotation of aromatic rings of AIE-active fluorogens, thereby effectively enhancing their AIE effect. Development of new supramolecularly enhanced AIE-based cancer cell imaging agents will not only allow for the clinical diagnoses and

prognoses of cancers but might also be helpful for the selective delivery of anticancer drugs.

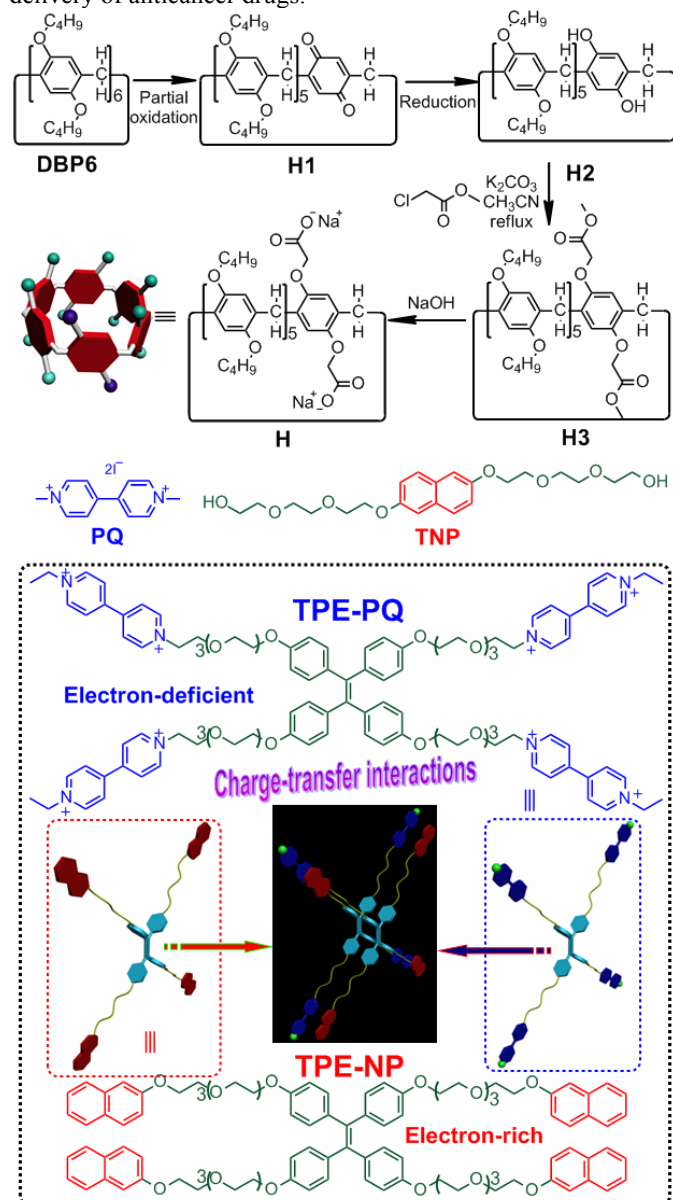


Fig. 1 Top: synthetic route to difunctional pillar[6]arene **H**. Middle: chemical structures of model compounds **PQ** and **TNP**. Bottom: chemical structures and cartoon representations of **TPE-PQ** and **TPE-NP**.

Herein, two four-armed TPE-based derivatives containing electron-rich naphthalene (**TPE-NP**) and electron-deficient paraquat (**TPE-PQ**) groups, respectively, were designed and synthesized. Charge-transfer (CT) interactions between the electron-rich naphthyl groups and electron-deficient paraquat units were achieved,⁸ resulting in the restriction of the intramolecular rotation of the benzene rings to enhance the emission significantly. **TPE-NP** and **TPE-PQ** self-assembled into 1D nanorods in water driven by the CT interactions and the length of the self-assemblies could be controlled by adjusting the molar ratio between these two building blocks. On account of the existence of highly toxic paraquat groups, a difunctional negatively charged water-soluble pillar[6]arene **H** was employed to wrap the paraquat unit to reduce its toxicity and

enhance the membrane permeability of **TPE-PQ** through host-guest interactions.⁹ A ternary system containing **H**, **TPE-NP** and **TPE-PQ** was utilized as an imaging agent for cancer cells, due to the pH-responsiveness of **H**, **TPE-PQ** dethreaded from the cavity of **H** and formed a CT complex with **TPE-NP** in the breast cancer cells (MCF-7) with relatively low pH, thereby imaging the cancer cells.

Experimental section

Synthesis

The synthetic route to **H** is shown in Figure 1 and the synthetic routes to **TPE-PQ** and **TPE-NP** are shown in Scheme 1.

Synthesis of H1: A solution of 1,4-bis(butoxy)pillar[6]arene (**DBP6**)¹⁰ (5.62 g, 4.00 mmol) in THF (100 mL) was stirred while an aqueous solution of $(\text{NH}_4)_2[\text{Ce}(\text{NO}_3)_6]$ (2.19 g, 4.00 mmol) was added dropwise. The mixture was stirred at room temperature for 24 h. The organic solvent was removed and the water layer was extracted with dichloromethane (3×50 mL). The combined organic phase was washed with water (3×100 mL) and saturated NaCl solution (100 mL) and dried over anhydrous Na_2SO_4 . After filtration and evaporation, the residue was purified by column chromatography on silica gel (petroleum ether/dichloromethane, 4:1 \rightarrow 2:1 v/v) to provide **H1** as a red solid (640 mg, 21%), m.p. 129.1–130.8 °C. The ¹H NMR spectrum of **H1** is shown in Figure S1. ¹H NMR (400 MHz, chloroform-*d*, room temperature) δ (ppm): 6.82 (s, 2H), 6.77 (s, 2H), 6.75 (s, 2H), 6.71 (s, 2H), 6.68 (s, 2H), 6.43 (s, 2H), 3.90–3.73 (m, 28H), 3.61 (s, 4H), 1.80–1.73 (m, 20H), 1.54–1.49 (m, 20H), 1.02–0.92 (m, 30H). The ¹³C NMR spectrum of **H1** is shown in Figure S2. ¹³C NMR (100 MHz, chloroform-*d*, room temperature) δ (ppm): 187.17, 170.10, 149.60, 149.52, 149.49, 149.43, 149.38, 145.77, 132.43, 128.26, 127.17, 126.94, 126.15, 121.55, 114.31, 113.91, 113.80, 113.43, 67.31, 67.26, 67.04, 66.66, 59.36, 30.89, 30.86, 30.82, 30.39, 29.87, 29.33, 29.26, 20.00, 18.44, 18.42, 18.39, 18.33, 18.23, 13.17, 12.97, 12.92, 12.88, 12.64. LRESIMS: m/z 1314.3 [$\text{M} + \text{Na}$]⁺ (100%). HRESIMS: m/z calcd for [$\text{M} + \text{Na}$]⁺ $\text{C}_{82}\text{H}_{116}\text{O}_{12}\text{Na}$, 1315.8363, found 1315.8386, error 1.7 ppm.

Synthesis of H3: A solution of **H1** (702 mg, 0.500 mmol) in CH_2Cl_2 (20 mL) was stirred while an aqueous solution of $\text{Na}_2\text{S}_2\text{O}_4$ (1.92 g, 11.1 mmol) was added. The mixture was stirred at room temperature for 12 h. The water layer was extracted with CH_2Cl_2 (3×50 mL). The combined organic phase was washed with water (3×100 mL) and saturated NaCl solution (100 mL) and dried over anhydrous Na_2SO_4 . After filtration and evaporation, the resulting **H2** was used in the next step without further purification. Methyl chloroacetate (2.59 g, 24.0 mmol) and K_2CO_3 (6.62 g, 48.0 mmol) were added to a solution of **H2** (645 mg, 0.500 mmol) in CH_3CN (50 mL). The mixture was heated under nitrogen at reflux for 12 h. The cooled reaction mixture was filtered and washed with chloroform. The filtrate was evaporated under vacuum, and the residue was purified by flash column chromatography (dichloromethane/ethyl acetate, 20:1 v/v) to yield **H3** as a white solid (689 mg, 96%), m.p. 146.5–148.2 °C. The proton NMR spectrum of **H3** is shown in Figure S5. ¹H NMR (400 MHz, chloroform-*d*, room temperature) δ (ppm): 6.86 (s, 2H), 6.73 (s, 2H), 6.71 (s, 2H), 6.68 (s, 2H), 6.66 (s, 4H), 4.37 (s, 4H), 3.82–3.71 (m, 38H), 1.72–1.63 (m, 20H), 1.45–1.41 (m, 20H), 1.30–1.26 (m, 30H). The ¹³C NMR spectrum of **H3** is shown in Figure S6. ¹³C NMR (100 MHz, chloroform-*d*, room

temperature) δ (ppm): 168.53, 149.49, 149.47, 149.44, 149.38, 149.17, 127.79, 127.05, 126.92, 126.87, 126.67, 126.02, 114.58, 114.09, 114.00, 113.83, 113.64, 76.36, 76.04, 75.72, 67.22, 67.12, 66.99, 65.27, 50.77, 30.90, 30.87, 30.84, 30.82, 30.01, 29.64, 29.53, 28.68, 18.43, 18.39, 18.37, 18.33, 12.92, 12.90, 12.88, 12.86, 12.78. LRESIMS is shown in Figure S7: m/z 1459.3 $[M + Na]^+$ (100%). HRESIMS: m/z calcd for $[M + K]^+$ $C_{88}H_{124}O_{16}Na$, 1459.8787, found 1459.8763, error -1.6 ppm.

Synthesis of H: A solution of **H3** (718 mg, 0.500 mmol) in CH_3CH_2OH (40 mL) was treated with 40% aqueous sodium hydroxide (40 mL) at reflux for 12 h. The mixture was concentrated under reduced pressure, and diluted with water (10 mL). The precipitate was collected by filtration, washed with water, and dried under vacuum to give **H** (727 mg, 100%) as a white solid, m.p. 167.5–169.8 °C. The proton NMR spectrum of **H** is shown in Figure S8. 1H NMR (400 MHz, chloroform-*d*, room temperature) δ (ppm): 7.06 (s, 2H), 6.74 (s, 2H), 6.69 (s, 4H), 6.65 (s, 2H), 6.59 (s, 2H), 4.31 (s, 4H), 3.89–3.67 (m, 32H), 1.70–1.61 (m, 20H), 1.44–1.31 (m, 20H), 0.90–0.78 (m, 30H). The ^{13}C NMR spectrum of **H** is shown in Figure S9. ^{13}C NMR (100 MHz, chloroform-*d*, room temperature) δ (ppm): 169.63, 150.50, 150.45, 150.39, 150.17, 128.78, 128.07, 127.92, 127.87, 127.66, 127.00, 115.60, 115.13, 115.01, 114.85, 114.65, 68.24, 68.14, 68.00, 66.28, 51.85, 31.91, 31.88, 31.82, 31.06, 30.56, 19.45, 19.41, 19.39, 19.35, 13.96, 13.94, 13.90, 13.82. LRESIMS is shown in Figure S10: m/z 1491.0 $[M + K]^+$ (100%). HRESIMS: m/z calcd for $[M - Na]^+$ $C_{86}H_{119}O_{16}$, 1407.8498, found 1407.8523, error 1.7 ppm.

Synthesis of 3: **2** (20.9 g, 60.0 mmol) and K_2CO_3 (13.2 g, 98.0 mmol) were added to a solution of **1** (3.96 g, 10.0 mmol) in CH_3CN (300 mL). The mixture was heated in a three-necked flask under nitrogen atmosphere at reflux for 2 d. The cooled reaction mixture was filtered and washed with chloroform. The filtrate was evaporated under vacuum, and the residue was used in the next step without further purification. To a solution of the crude product and 4-toluenesulphonyl chloride (19.1 g, 100 mmol) in dichloromethane (200 mL), triethylamine (20 mL) was added dropwise at 0 °C. Then the mixture was stirred at room temperature for 12 h. The mixture was washed with water (3×10 mL) and the solvent was removed under reduced pressure to give the crude product, which was purified by flash column chromatography (dichloromethane/ethyl acetate, 9:1 *v/v*) to yield **3** as a light red oil (7.89 g, 46%). The proton NMR spectrum of **3** is shown in Figure S14. 1H NMR (400 MHz, chloroform-*d*, room temperature) δ (ppm): 7.79 (d, $J = 8$ Hz, 8H), 7.33 (d, $J = 8$ Hz, 8H), 6.89 (d, $J = 8$ Hz, 8H), 6.62 (d, $J = 8$ Hz, 8H), 4.15 (d, $J = 4$ Hz, 5H), 4.04 (d, $J = 4$ Hz, 8H), 3.80 (d, $J = 4$ Hz, 8H), 3.70–3.66 (m, 16H), 3.64–3.60 (m, 16H), 3.58 (s, 20H). The ^{13}C NMR spectrum of **3** is shown in Figure S15. ^{13}C NMR (100 MHz, chloroform-*d*, room temperature) δ (ppm): 156.99, 144.81, 138.37, 137.00, 133.02, 132.49, 129.83, 127.98, 113.67, 70.74, 70.64, 70.53, 69.76, 69.26, 68.67, 67.17, 21.64. LRESIMS is shown in Figure S16: m/z 1734.6 $[M + NH_4]^+$ (100%). HRESIMS: m/z calcd for $[M + H]^+$ $C_{86}H_{109}O_{28}S_4$, 1717.5988, found 1717.6011, error 1 ppm.

Synthesis of TPE-NP: 2-Naphthol (2.88 g, 20.0 mmol) and K_2CO_3 (13.8 g, 100 mmol) were added to a solution of **3** (3.43 g, 2.00 mmol) in CH_3CN (50 mL). The mixture was heated under nitrogen at reflux for 2 d. The cooled reaction mixture was filtered and washed with chloroform. The filtrate was evaporated under vacuum, and the residue was purified by flash column chromatography (dichloromethane/ethyl acetate, 9:1 *v/v*) to yield **TPE-NP** as a light red oil (2.18 g, 68%). The proton NMR spectrum of **TPE-NP** is shown in Figure S17. 1H NMR

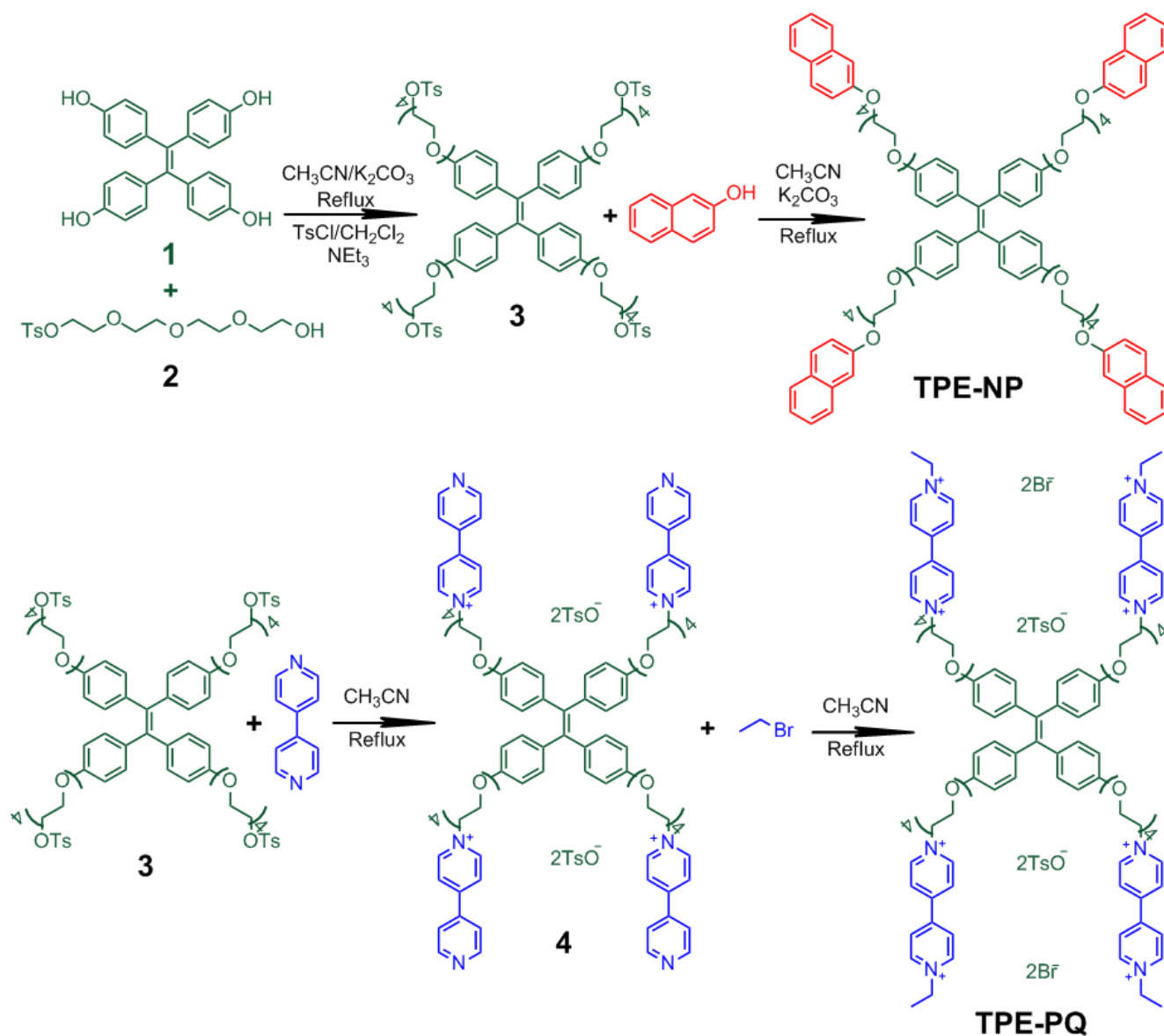
(400 MHz, chloroform-*d*, room temperature) δ (ppm): 7.75–7.69 (m, 12H), 7.41 (td, $J_1 = 8$ Hz, $J_2 = 1$ Hz, 4H), 7.31 (td, $J_1 = 8$ Hz, $J_2 = 1$ Hz, 4H), 7.16 (dd, $J_1 = 8$ Hz, $J_2 = 4$ Hz, 4H), 7.12 (d, $J = 4$ Hz, 4H), 6.87 (d, $J = 8$ Hz, 8H), 6.60 (d, $J = 8$ Hz, 8H), 4.23 (t, $J = 4$ Hz, 8H), 4.00 (t, $J = 4$ Hz, 8H), 3.90 (d, $J = 4$ Hz, 8H), 3.79–3.76 (m, 8H), 3.75–3.72 (m, 8H), 3.70–3.67 (m, 24H). The ^{13}C NMR spectrum of **TPE-NP** is shown in Figure S18. ^{13}C NMR (100 MHz, chloroform-*d*, room temperature) δ (ppm): 156.99, 156.76, 138.36, 136.99, 134.50, 132.51, 129.39, 129.02, 127.65, 126.78, 126.36, 123.66, 119.05, 113.67, 106.73, 70.88, 70.79, 70.70, 69.77, 69.74, 67.43, 67.15. LRESIMS is shown in Figure S19: m/z 1623.8 $[M + H_3O]^+$ (100%). HRESIMS: m/z calcd for $[M + H]^+$ $C_{98}H_{109}O_{20}$, 1605.7512, found 1605.7526, error 0.8 ppm.

Synthesis of 4: 4,4'-Bipyridine (9.36 g, 60.0 mmol) was added to a solution of **3** (3.43 g, 2.00 mmol) in CH_3CN (500 mL). The mixture was heated under nitrogen at reflux for 2 d. The cooled reaction mixture was evaporated under vacuum, and the residue was purified by flash column chromatography (from dichloromethane/methanol (6:1 *v/v*) to $MeOH/NH_4Cl$ (2 N)/ $MeNO_2$ (7:2:1 *v/v/v*) to yield **4** as a light red oil (1.45 g, 32%). The proton NMR spectrum of **4** is shown in Figure S20. 1H NMR (400 MHz, D_2O , room temperature) δ (ppm): 8.86 (s, 8H), 8.18 (s, 8H), 7.66 (s, 8H), 8.86 (s, 8H), 7.42 (d, $J = 4$ Hz, 4H), 6.87 (d, $J = 8$ Hz, 4H), 6.53 (s, 16H), 6.27 (s, 16H), 3.93 (s, 12), 3.63–3.40 (m, 64H). The ^{13}C NMR spectrum of **4** is shown in Figure S21. ^{13}C NMR (100 MHz, D_2O , room temperature) δ (ppm): 156.54, 153.21, 149.91, 146.10, 145.46, 141.03, 140.90, 138.37, 136.68, 132.23, 129.14, 126.67, 125.49, 122.55, 113.75, 69.88, 69.57, 68.92, 68.66, 67.00, 60.85, 60.39, 46.70, 20.63. LRESIMS is shown in Figure S22: m/z 1255.9 $[M + TsO - H]^2-$ (100%). HRESIMS: m/z calcd for $[M - 4TsO]^4+$ $C_{98}H_{112}N_8O_{16}$, 414.2049, found 414.2056, error 1.7 ppm.

Synthesis of TPE-PQ: Bromoethane (10.8 g, 100 mmol) was added to a solution of **4** (2.34 g, 1.00 mmol) in CH_3CN (50 mL). The mixture was heated under nitrogen at reflux for 12 h. The cooled reaction mixture was evaporated under vacuum to yield **TPE-PQ** as a light red oil (2.77 g, 100%). The proton NMR spectrum of **TPE-PQ** is shown in Figure S23. 1H NMR (400 MHz, D_2O , room temperature) δ (ppm): 8.99 (s, 16H), 8.35 (s, 16H), 6.86–6.51 (m, 32H), 4.78 (s, 8H), 4.60 (t, $J = 8$ Hz, 8H), 3.96–3.90 (m, 16H), 3.56–3.51 (m, 53H), 1.56 (t, $J = 4$ Hz, 12H). The ^{13}C NMR spectrum of **TPE-PQ** is shown in Figure S24. ^{13}C NMR (100 MHz, D_2O , room temperature) δ (ppm): 146.07, 145.97, 145.20, 145.16, 132.26, 132.09, 129.34, 126.94, 126.89, 126.74, 126.71, 126.67, 126.64, 125.38, 113.94, 69.89, 69.73, 69.66, 69.54, 68.91, 68.58, 67.19, 61.32, 57.68, 20.49, 15.62. LRESIMS is shown in Figure S25: m/z 874.6 $[M + TsO - 4Br]^3+$ (100%). HRESIMS: m/z calcd for $[M - 4TsO - 4Br]^8+$ $C_{106}H_{132}N_8O_{16}$, 221.6220, found 221.6227, error 3.2 ppm.

Cell Culture

MCF-7 and HEK293 cells were cultured in Dulbecco's modified Eagle's medium (DMEM) containing 10% fetal bovine serum (FBS) and 1% penicillin/streptomycin. Cells grew as a monolayer and were detached upon confluence using trypsin (0.5% *w/v* in PBS). The cells were harvested from cell culture medium by incubating in trypsin solution for 5 min. The cells were centrifuged, and the supernatant was discarded. A 3 mL portion of serum-supplemented DMEM was added to neutralize any residual trypsin. The cells were resuspended in serum-supplemented DMEM at a concentration of 1×10^4 cells/mL. Cells were cultured at 37 °C and 5% CO_2 .



Scheme 1. Synthetic routes to TPE-PQ and TPE-NP.

Evaluation of Cytotoxicity

The cytotoxicity of **H**, **TPE-NP**, **TPE-PQ**, **TPE-PQ@TPE-NP** and **H₄⊃TPE-PQ** against MCF-7 and HEK293 cells were determined by 3-(4,5-dimethylthiazol-2-yl)-2,5-diphenyl tetrazolium bromide (MTT) assay in a 96-well cell culture plate. All solutions were sterilized by filtration with a 0.22 μm filter before tests. Raw 264.7 cells were seeded at a density of 1×10^4 cells/well in a 96-well plate, and incubated for 24 h for attachment. Cells were then incubated with **H**, **TPE-NP**, **TPE-**

PQ, **TPE-PQ@TPE-NP** and **H₄⊃TPE-PQ** at various concentrations for 4 h and 24 h, respectively. Then 20 μL of a MTT solution (5 mg/mL) was added to each well. After 4 h of incubation at 37 °C, the MTT solution was removed, and the insoluble formazan crystals that formed were dissolved in 100 μL of dimethylsulfoxide (DMSO). The absorbance of the formazan product was measured at 570 nm using a spectrophotometer (Bio-Rad Model 680). Untreated cells in media were used as a control. All experiments were carried out with three replicates.

Results and discussion

Supramolecular Enhancement of Aggregation-Induced Emission Driven by Charge-Transfer Interactions

TPE-NP exhibits the characteristic AIE feature. It gives very weak emission in THF where it is well dissolved with the wavelength of emission bands at 386 and 412 nm corresponding to the emission of naphthalene rings. Water is a poor solvent for **TPE-NP** due to the existence of highly hydrophobic aromatic rings of **TPE-NP**. As shown in Fig. S32, the fluorescence intensity (FL) of **TPE-NP** was enhanced gradually by increasing the volume fraction of water (f_w) in the THF/H₂O mixture from 0 to 80 vol%, accompanied by a red-shift to 491 nm for the emission maximum. Moreover, the FL intensity of **TPE-NP** at 491 nm increased dramatically upon further enhancement of f_w from 80 to 90 vol%, 44-fold as compared to that in the pure THF solution, consistent with other hydrophobic AIE dyes. On the contrary, **TPE-PQ** shows excellent solubility (higher than 50 mM) in water due to the presence of four dicationic paraquat units as arms, resulting in the failure of the AIE effect in water. As shown in Fig. 2b, the fluorescence intensity of **TPE-PQ** was almost unchanged with increasing concentration from 0 to 30 μ M in water. The reason was that **TPE-PQ** dissolved in water easily, and the intramolecular rotation of the aromatic rings in the TPE group could not be restricted, thereby invalidating its AIE effect.

The charge-transfer complex **TPE-PQ@TPE-NP** was prepared by mixing equivalent amounts of **TPE-NP** and **TPE-PQ** in a mixture of THF and CH₃OH (1:1 v/v), which is a good solvent for both **TPE-NP** and **TPE-PQ**. The solvent was then removed under reduced pressure, and the dissolution-evaporation procedure was repeated five times to ensure complete complexation between **TPE-NP** and **TPE-PQ**. The preassembled CT complex **TPE-PQ@TPE-NP** showed excellent solubility in water, yielding a light red transparent solution which was stable for several weeks. Since uncomplexed **TPE-NP** is insoluble in water, the enhancement in the solubility of **TPE-NP** with **TPE-PQ** must be attributed to the successful formation of the CT complex.^{8a} Interestingly, the FL intensity at 491 nm of the aqueous solution containing **TPE-PQ@TPE-NP** increased gradually by increasing the concentration of the CT complex (Fig. 2b). Notably, the FL intensity of **TPE-NP** was higher than that of **TPE-PQ@TPE-NP** at the same concentration when the TPE concentration was lower than 12 μ M, while the FL intensity of **TPE-NP** was surpassed by that of **TPE-PQ@TPE-NP** when the TPE concentration was higher than 12 μ M. On the other hand, the FL intensity changed slowly when the concentration of **TPE-NP** was higher than 8 μ M. The reason was that the solubility of **TPE-NP** was much poorer than that of the CT complex, and the intramolecular rotation of the aromatic rings was restricted effectively in water, resulting in the appearance of AIE effect, which made a greater contribution to the fluorescence enhancement than that of CT interactions between **TPE-PQ** and **TPE-NP** at low concentration (<12 μ M). However, the CT interactions restricted the rotation of the aromatic rings more effectively in solution when the concentration of the TPE group was higher than 12 μ M. Considering these two factors, the FL intensity of the CT complex exceeded that of **TPE-NP** at relatively high concentration (>12 μ M).

Direct evidence for the successful formation of the CT complex between **TPE-NP** and **TPE-PQ** was obtained from ¹H NMR spectroscopy (Fig. S33) using paraquat (**PQ**) and **TNP** as model compounds (Fig. 1, middle) due to the relatively poor

solubility of **TPE-NP**. Compared with the spectrum of **TNP** (Fig. S33c), the resonance peaks related to protons H_{1b}, H_{2b}, and H_{3b} on the naphthyl ring of **TNP** displayed upfield shifts ($\Delta\delta = -0.040$, -0.043 , and -0.046 ppm for H_{1b}, H_{2b}, and H_{3b}, respectively) in the presence of 3 equivalents of **PQ** (Fig. S33b). On the other hand, upfield shifts for the signals corresponding to protons H_{4b-9b} were observed as well, indicating the formation of a CT complex between **PQ** and **TNP**.^{8b} Furthermore, cyclic voltammetry (CV) experiments were carried out to provide convincing insight into the CT interactions between **TPE-NP** and **TPE-PQ** (Fig. S34). Compared with free **PQ**, the reduction and oxidation potentials had dramatic changes in the presence of equimolar **TNP** due to the formation of the CT complex.

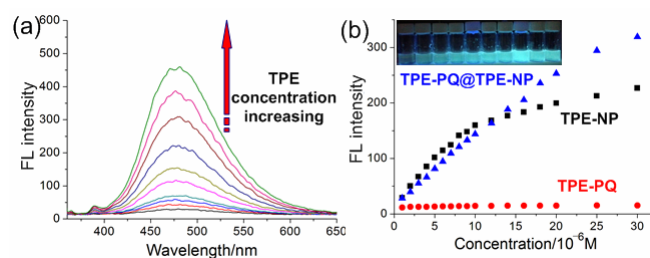


Fig. 2 (a) Fluorescence spectra of **TPE-PQ@TPE-NP** at different TPE concentrations in water at room temperature. (b) Plot of emission intensity at 491 nm vs. the TPE concentration. The inset in (b) is a fluorescent photo of **TPE-PQ@TPE-NP** in water at different TPE concentrations.

Self-Assembly of the Charge-Transfer Complex

Due to the propeller-shaped structure of TPE and the dynamic rotation of the phenyl rings, the self-assembly of TPE-based building blocks has been rarely reported due to the failure of π - π stacking without introduction of other driving forces.¹⁰ After the establishment of the CT complex **TPE-PQ@TPE-NP** in water as a supra-amphiphile,^{8c} we wondered whether these building blocks would self-assemble to interesting nanostructures on account of the introduction of the CT interactions between the electron-rich naphthalene rings and electron-deficient paraquat units. Two possible packing modes might be achieved for **TPE-NP** and **TPE-PQ** driven by CT interactions: one-dimensional (1D) self-assembly and two-dimensional (2D) self-assembly as shown in Fig. S36. Transmission electron microscopy (TEM) was employed to reveal the morphology of the self-assembly. As shown in Fig. 3, nanorods were observed with ~ 6 nm diameter and ~ 1 μ m length after a solution containing equimolar **TPE-NP** and **TPE-PQ** stood for two weeks. From a magnified image of these nanostructures (Fig. 3c), no sharp color contrast between the periphery and central parts was noted, indicating that the one dimensional nanostructures were solid nanorods (rod-like micelles). Notably, the nanorods were quite straight and smooth, which was attributed to the existence of cationic paraquat groups on the surfaces of the nanorods, generating electrostatic repulsive interactions. Interestingly, the average length of the nanorods decreased to ~ 300 nm when the **TPE-PQ/TPE-NP** molar ratio was changed to 50/49 (Fig. 3d), and it further decreased to ~ 200 nm at a molar ratio of 50/45 (Fig. 3f). The reason was that excess **TPE-PQ** in the solution acted as stoppers to inhibit the growth of the nanorods, resulting in the reduction of their length.

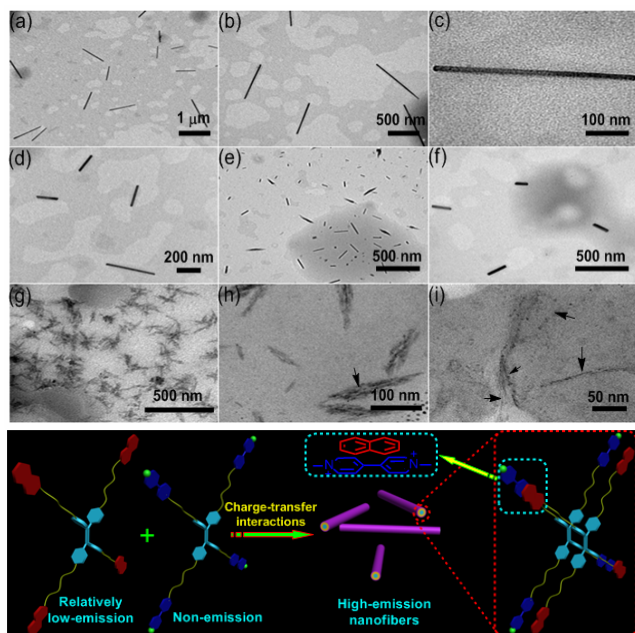


Fig. 3 TEM images: (a) TPE-PQ@TPE-NP (the TPE concentration is 2.00×10^{-5} M, TPE-PQ/TPE-NP = 1/1); (b) enlarged image of (a) (scale bar = 500 nm); (c) enlarged image of (a) (scale bar = 100 nm); (d) TPE-PQ@TPE-NP (the TPE concentration is 2.00×10^{-5} M, TPE-PQ/TPE-NP = 50/49); (e) TPE-PQ@TPE-NP (the TPE concentration is 2.00×10^{-5} M, TPE-PQ/TPE-NP = 50/45); (f) enlarged image of (e); (g) TPE-PQ@TPE-NP (the TPE concentration is 5.00×10^{-4} M, TPE-PQ/TPE-NP = 1/1); (h) enlarged image of (g) (scale bar = 100 nm); (i) enlarged image of (g) (scale bar = 50 nm). Schematic representation of the self-assembly process of TPE-PQ and TPE-NP driven by charge-transfer interactions.

Furthermore, the nanorods formed bundles with lengths of ~ 300 nm when the concentration of the building blocks was increased to 5.00×10^{-4} M (Fig. 3g–3i), and the diameter of the self-assemblies remained ~ 6 nm. Due to the existence of electron-rich naphthalene rings and electron-deficient paraquat units on the surfaces of the nanorods, CT interactions between the nanorods resulted in the formation of relatively larger aggregates. It should be noted that the extended length of the building blocks is about 6 nm (Fig. S35) which is close to the diameter of the nanorods, suggesting face-to-face packing of TPE-NP and TPE-PQ. On the other hand, no increase in viscosity was observed with increased concentration, indicating that the CT complex indeed self-assembled in water in 1D packing mode (Fig. 3). A mechanism to explain why the CT complex self-assembled into 1D nanorods rather than 2D aggregates, relates to the hydrophobic TPE regions adhering to the neighboring ones to minimize the exposure of the hydrophobic regions to water.¹¹ As mentioned above, the AIE effect was enhanced significantly by the formation of the CT complex, resulting in restriction of intramolecular rotation of the aromatic rings on the TPE groups in the core of the nanorods.

pH-Responsive Complexation between H and TPE-PQ

Compared with TPE-NP, paraquat derivatives exhibited high toxicity for the cells due to increased intracellular levels of superoxide ($O_2^{\cdot-}$), which limits their bio-relevant applications. Pillar[*n*]arenes, mainly including pillar[5]arenes¹² and pillar[6]arenes,¹³ a new kind of macrocyclic hosts next to crown ethers, cyclodextrins, calixarenes, and cucurbiturils,¹⁴ are linked

by methylene ($-CH_2-$) bridges at *para*-positions of 2,5-dialkoxybenzene rings, forming unique rigid pillar architectures. The unique symmetrical structure and easy functionalization of pillararenes have afforded them superior properties in host-guest recognition. Pillararenes act as useful platforms for the construction of various interesting supramolecular systems, including liquid crystals,^{13g} cyclic dimers,^{15a,e} chemosensors,^{15b,f} supramolecular polymers,^{15c,g,h} drug delivery systems,^{15k} transmembrane channels,^{15d,j} cell glue^{15l} and selective adsorption porous material.^{15m} From our previous work, we knew that pillar[6]arenes formed stable inclusion complexes with paraquat, reducing the toxicity of PQ effectively.⁹ On account of these factors, a difunctional pillar[6]arene **H** bearing two anionic carboxylate groups was designed and synthesized to effectively wrap the toxic paraquat groups on TPE-PQ through host-guest interactions to form electroneutral complexes.¹⁶

Driven by the cooperativity of electrostatic interactions, hydrophobic interactions, and π - π stacking interactions between cationic paraquat units and anionic **H**, a stable host-guest complex $H_4 \supset TPE-PQ$ formed (see ESI, Fig. S37–S39). The association constant between paraquat and **H** was $(4.54 \pm 0.19) \times 10^3$ M⁻¹, indicating that the complex $H_4 \supset TPE-PQ$ was quite stable in water (Fig. S39). Moreover, the assembly and disassembly between **H** and TPE-PQ could be reversibly controlled by sequential addition of aqueous DCI and NaOD due to the pH-responsiveness of **H** (Fig. S40). When the solution became acidic, the carboxylate groups on **H** were protonated into carboxylic acid groups, resulting in the disassociation of the complex.⁹ Upon addition of NaOD, the carboxylic acid groups were deprotonated to anionic carboxylate groups, which interacted with the cationic guest effectively again to form a stable inclusion complex. The pH-responsive complexation between **H** and TPE-PQ was accompanied with FL intensity changes. Compared with free TPE-PQ exhibiting weak emission, a significant FL enhancement was observed upon formation of an electroneutral host-guest complex $H_4 \supset TPE-PQ$, which showed relatively poor solubility in water, thus inducing the appearance of the AIE effect. On the contrary, TPE-PQ was dethreaded from the cavity of **H** and dissolved in water freely by protonation of the pH-responsive macrocyclic host, resulting in the reversal of the AIE effect (Fig. S41).

Host-Induced Toxicity Reduction and Application of the Ternary Supramolecular System in Living Cancer Cell Imaging

In order to further apply these supramolecular systems in biologically and pharmaceutically relevant fields, their toxicity needed to be evaluated. A simple evaluation of cytotoxicity for **H**, TPE-NP, TPE-PQ, TPE-PQ@TPE-NP and the host-guest complex $H_4 \supset TPE-PQ$ at different concentrations against MCF-7 and HEK293 cells was carried out by using a 3-(4',5'-dimethylthiazol-2'-yl)-2,5-diphenyltetrazolium bromide (MTT) assay. Fig. 4a–4d show the minimal influence on cell viability and proliferation for both MCF-7 and HEK293 cells incubated with **H** and TPE-NP for 4 h and 24 h with the concentration ranging from 20 to 150 μ g mL⁻¹, indicating the excellent biocompatibility and low toxicity of these two compounds. On the other hand, TPE-PQ exhibited high toxicity against MCF-7 and HEK293 cells; the addition of TPE-PQ led to rapid decrease in relative cell viability. In stark contrast, the relative cell viability of the host-guest complex $H_4 \supset TPE-PQ$ was

higher than that of **TPE-PQ** at the same concentration, which indicated that the toxicity of **TPE-PQ** was significantly reduced upon formation of the stable host-guest complex.

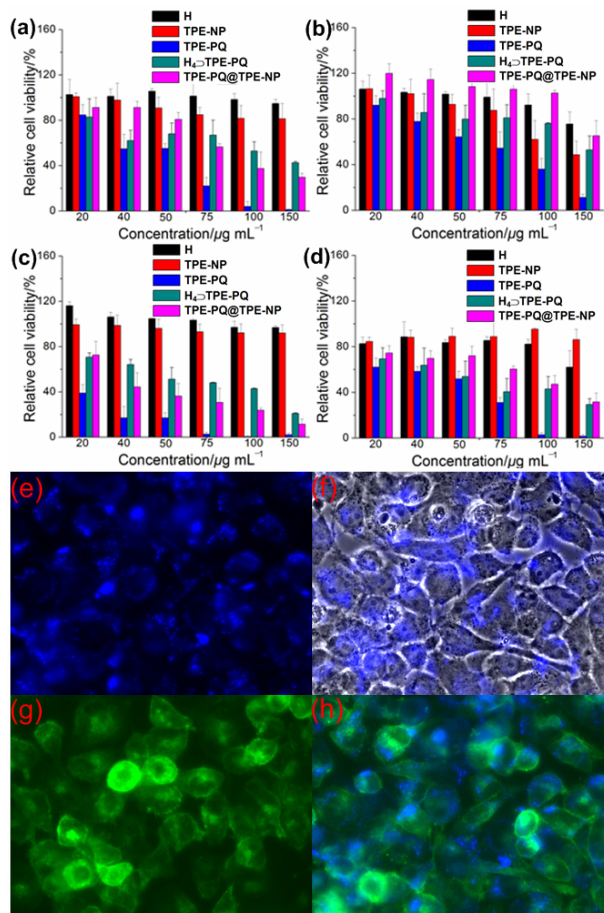


Fig. 4 Relative cell viabilities of (a) MCF-7 cells (4 h), (b) HEK293 cells (4 h), (c) MCF-7 cells (24 h), and (d) HEK293 cells (24 h) incubated with **H**, **TPE-NP**, **TPE-PQ**, **TPE-PQ@TPE-NP** and the host-guest complex **H₄⊃TPE-PQ** at different concentrations. Confocal images of live MCF-7 breast cancer cells after incubation with **H₄⊃TPE-PQ@TPE-NP** (**H**, **TPE-PQ**, and **TPE-NP** concentrations are 1.00×10^{-4} M, 2.50×10^{-5} M, and 2.50×10^{-5} M, respectively) for 2 h: (e) fluorescent image; (f) merged image from (e) and the bright field image; (g) stained with FITC; (h) merged image from (e) and (g).

From our previous work,⁹ we knew that the redox process of **TPE-PQ** was inhibited by forming a stable inclusion complex with **H**, which makes the generation of the radical cations more difficult, resulting in a decrease of the concentration of toxic HO[•]. Interestingly, the toxicity of the CT complex **TPE-PQ@TPE-NP** was also lower than that of **TPE-PQ** at the same concentration. The reason was that the reduction and oxidation potentials of paraquat were impacted dramatically in the presence of electron-rich **TPE-NP**, which was demonstrated by CV experiments mentioned above (Fig. S34), making the generation of the toxic HO[•] more difficult. It should be noted that the toxicity of **H₄⊃TPE-PQ** against the cancer cells MCF-7 was higher than that against HEK293 cells. Because the pH value in cancer cells was lower than that in normal cells, the toxic paraquat units on **TPE-PQ** were dethreaded from the cavity of **H** that was protonated in the relatively acidic environment, resulting in the enhancement of toxicity to the cancer cells.

Furthermore, a ternary supramolecular system containing **H**, **TPE-NP** and **TPE-PQ** was utilized as a living cell imaging agent. The electroneutral **H₄⊃TPE-PQ** was uptaken by MCF-7 cells relatively easily compared with positively charged **TPE-PQ**. **H₄⊃TPE-PQ** disassembled in the cell by protonation of pH-responsive **H** into the neutral state. Then the electron-deficient paraquat groups on **TPE-PQ** dethreaded from the cavity of **H** and interacted with electron-rich naphthalene rings on **TPE-NP** to form a stable CT complex in the cells, resulting in the enhanced AIE due to the restriction of the intramolecular rotation of the aromatic rings on TPE groups. This enhanced AIE was applied in cell imaging. The CT complex stained cells showed a bright densely punctuated pattern in the cytoplasm by confocal fluorescence microscopy with excitation wavelength $\lambda = 405$ nm. In our studies, we found that this ternary supramolecular system could not stain normal cells due to the relatively high pH value in these cells. This relatively high pH value meant that the disassembly of **H₄⊃TPE-PQ** could not be easily achieved, efficiently hindering the formation of the AIE-enhanced CT complex **TPE-PQ@TPE-NP**.

Conclusions

In summary, two tetraphenylethene derivatives containing electron-rich naphthalene (**TPE-NP**) and electron-deficient paraquat (**TPE-PQ**) groups, respectively, were designed and synthesized. Driven by charge-transfer (CT) interactions, **TPE-NP** and **TPE-PQ** self-assembled into nanorods in 1D packing mode, resulting in the restriction of intramolecular rotation to enhance the aggregation-induced emission (AIE) effect significantly. In order to enhance the membrane permeability and reduce the toxicity of **TPE-PQ**, a difunctional pillar[6]arene **H** bearing two carboxylate anionic groups was employed to form pH-responsive inclusion complexes with the four paraquat units of **TPE-PQ**. Due to the pH-responsiveness of **H**, a ternary supramolecular system containing **H**, **TPE-NP** and **TPE-PQ** was utilized as a living cell imaging agent, which stained the cancer cells. In the cancer cells, **TPE-PQ** dethreaded from the cavity of **H**, and interacted with **TPE-NP** to form a stable CT complex, resulting in the restriction of the intramolecular rotation of the aromatic rings on TPE groups to induce the appearance of an enhanced AIE phenomenon in the cytoplasm. These results indicate that the combination of the AIE effect and supramolecular chemistry has enormous potential in biologically and pharmaceutically relevant fields, such as biosensors, drug and gene delivery systems, protein-protein interactions and cell imaging.

Acknowledgements

This work was supported by National Basic Research Program (2013CB834502) and the National Natural Science Foundation of China (21125417).

Notes and references

^a State Key Laboratory of Chemical Engineering, Department of Chemistry, Zhejiang University, Hangzhou 310027, P. R. China. E-mail: fhuang@zju.edu.cn; Fax: 86 571 8795 3189; Tel: 86 571 8795 3189

^b Department of Chemistry, Institute of Chemical Biology and Pharmaceutical Chemistry, Zhejiang University Hangzhou, 310027, P. R. China.

† Electronic Supplementary Information (ESI) available: [Synthetic procedures, characterizations]. See DOI: 10.1039/b000000x/

- 1 (a) S. R. Meech, *Chem. Soc. Rev.*, 2009, **38**, 2922; (b) P. Tanury, A. Malhotra, L. M. Byrne and S. Santra, *Adv. Drug Delivery Rev.*, 2010, **62**, 424; (c) G. M. van Dam, G. Themelis, L. M. A. Crane, N. J. Harlaar, R. G. Pleijhuis, W. Kelder, A. Sarantopoulos, J. S. de Jong, H. J. G. Arts, A. G. J. van der Zee, J. Bart, P. S. Low and V. Ntziachristos, *Nat. Med.*, 2011, **17**, 1315.
- 2 (a) I. L. Medintz, H. T. Uyeda, E. R. Goldman and H. Mattoussi, *Nat. Mater.*, 2005, **4**, 435; (b) M. De, P. S. Ghosh and V. M. Rotello, *Adv. Mater.*, 2008, **20**, 4225.
- 3 (a) J. Liu, J. W. Y. Lam and B. Z. Tang, *Chem. Rev.*, 2009, **109**, 5799; (b) K. Y. Pu and B. Liu, *Adv. Funct. Mater.*, 2009, **19**, 277.
- 4 (a) J. Luo, Z. Xie, J. W. Y. Lam, L. Cheng, H. Chen, C. Qiu, H. S. Kwok, X. Zhan, Y. Liu, D. Zhu and B. Z. Tang, *Chem. Commun.*, 2001, 1740; (b) J. Liu, J. W. Y. Lam and B. Z. Tang, *Chem. Rev.*, 2009, **109**, 5799; (c) Y. Mao, H. P. Xu, H. Zhao, W. Z. Yuan, A. Qin, Y. Yu, M. Faisal, Z. X. A, J. Z. Sun, and B. Z. Tang, *J. Mater. Chem.*, 2011, **21**, 13627; (d) Y. Hong, J. W. Y. Lam and B. Z. Tang, *Chem. Soc. Rev.*, 2011, **40**, 5361; (e) R. Hu, J. L. Maldonado, M. Rodriguez, C. Deng, C. K. W. Jim, J. W. Y. Lam, M. M. F. Yuen, G. Ramos-Ortiz and B. Z. Tang, *J. Mater. Chem.*, 2012, **22**, 232; (f) J. Mei, J. Wang, A. Qin, H. Zhao, W. Yuan, Z. Zhao, H. H. Y. Sung, C. Deng, S. Zhang, I. D. Williams, J. Z. Sun and B. Z. Tang, *J. Mater. Chem.*, 2012, **22**, 4290; (g) J. Wang, J. Mei, R. Hu, J. Z. Sun, A. Qin and B. Z. Tang, *J. Am. Chem. Soc.*, 2012, **134**, 9956; (h) D. Ding, K. Li, B. Liu and B. Z. Tang, *Acc. Chem. Res.*, 2013, **46**, 2441; (i) Z. Zhao, J. W. Y. Lam and B. Z. Tang, *Soft Matter*, 2013, **9**, 4564.
- 5 (a) J. Chen, C. C. W. Law, J. W. Y. Lam, Y. Dong, S. M. F. Lo, I. D. Williams, D. B. Zhu and B. Z. Tang, *Chem. Mater.*, 2003, **15**, 1535; (b) Q. Zhao, X. A. Zhang, Q. Wei, J. Wang, X. Y. Shen, A. Qin, J. Z. Sun and B. Z. Tang, *Chem. Commun.*, 2012, **48**, 11671; (c) S. Chen, J. Liu, Y. Liu, H. Su, Y. Hong, C. K. W. Jim, R. T. K. Kwok, N. Zhao, W. Qin, J. W. Y. Lam, K. S. Wong and B. Z. Tang, *Chem. Sci.*, 2012, **3**, 1804; (d) H. Shi, J. Liu, J. Geng, B. Z. Tang and B. Liu, *J. Am. Chem. Soc.*, 2012, **134**, 9569; (e) J. Geng, K. Li, D. Ding, X. Zhang, W. Qin, J. Liu, B. Z. Tang and B. Liu, *Small*, 2012, **8**, 3655; (f) G. Xu, Q. Xu, A. Qin, J. Cheng, N. Wang, J. Wei, C. Zhang, Z. Yang and B. Z. Tang, *J. Mater. Chem. C*, 2013, **1**, 1717; (g) W. Qin, K. Li, G. Feng, M. Li, Z. Yang, B. Liu and B. Z. Tang, *Adv. Funct. Mater.*, 2014, **24**, 635; (h) X. Yao, X. Ma and H. Tian, *J. Mater. Chem. C*, 2014, DOI: 10.1039/c4tc00503a.
- 6 (a) H. G. Sudibya, J. Ma, X. Dong, S. Ng, L.-J. Li, X.-W. Liu and P. Chen, *Angew. Chem. Int. Ed.*, 2009, **48**, 2723; (b) G. Yu, J. Li, W. Yu, C. Han, Z. Mao, C. Gao and F. Huang, *Adv. Mater.*, 2013, **25**, 6373.
- 7 (a) Y. Ma, S. V. Kolotuchin and S. C. Zimmerman, *J. Am. Chem. Soc.*, 2002, **124**, 13757; (b) S. C. Zimmerman, M. S. Wendland, N. A. Rakow, I. Zharov and K. S. Suslick, *Nature*, 2002, **418**, 399; (c) F. Huang, F. R. Fronczek and H. W. Gibson, *J. Am. Chem. Soc.*, 2003, **125**, 9272; (d) T. Han and C.-F. Chen, *Org. Lett.*, 2006, **8**, 1069; (e) L. Wang, Q. Chen, G.-B. Pan, L.-J. Wan, S. Zhang, X. Zhan, B. H. Northrop and P. J. Stang, *J. Am. Chem. Soc.*, 2008, **130**, 13433; (f) P. Yao, H. Wang, P. Chen, X. Zhan, X. Kuang, D. Zhu and M. Liu, *Langmuir*, 2009, **25**, 6633; (g) F. Rodler, J. Linders, T. Fenske, T. Rehm, C. Mayer and C. Schmuck, *Angew. Chem. Int. Ed.*, 2010, **49**, 8747; (h) G. Gröger, W. Meyer-Zaika, C. Böttcher, F. Gröhn, C. Ruthard and C. Schmuck, *J. Am. Chem. Soc.*, 2011, **133**, 8961; (i) Y. Chen, A. M. Kushner, G. A. Williams and Z. Guan, *Nat. Chem.*, 2012, **4**, 467; (j) J. Hentschel, A. M. Kushner, J. Ziller and Z. Guan, *Angew. Chem. Int. Ed.*, 2012, **51**, 10561; (k) H. W. Gibson, H. Wang, Z. Niu, C. Slebodnick, L. N. Zhakhov and A. L. Rheingold, *Macromolecules*, 2012, **45**, 1270. (l) A. V. Quathem, P. Lussis, D. A. Leigh, A.-S. Duwez and C.-A. Fustin, *Chem. Sci.*, 2014, **5**, 1449.
- 8 (a) X. Zhang and C. Wang, *Chem. Soc. Rev.*, 2011, **40**, 94; (b) F. Li, Q. Song, L. Yang, G. Wu and X. Zhang, *Chem. Commun.*, 2013, **49**, 1808.
- 9 G. Yu, X. Zhou, Z. Zhang, C. Han, Z. Mao, C. Gao and F. Huang, *J. Am. Chem. Soc.*, 2012, **134**, 19489.
- 10 (a) Z. Zhao, D. Liu, F. Mahtab, L. Xin, Z. Shen, Y. Yu, C. Y. K. Chan, P. Lu, J. W. Y. Lam, H. H. Y. Sung, I. D. Williams, B. Yang, Y. Ma and B. Z. Tang, *Chem. Eur. J.*, 2011, **17**, 5998; (b) X. Y. Shen, W. Z. Yuan, Y. Liu, Q. Zhao, P. Lu, Y. Ma, I. D. Williams, A. Qin, J. Z. Sun and B. Z. Tang, *J. Phys. Chem. C*, 2012, **116**, 10541; (c) Q. Zhao, K. Li, S. Chen, A. Qin, D. Ding, S. Zhang, Y. Liu, B. Liu, J. Z. Sun and B. Z. Tang, *J. Mater. Chem.*, 2012, **22**, 15128.
- 11 I.-H. Lee, P. Amaladas, K.-Y. Yoon, S. Shin, Y.-J. Kim, I. Kim, E. Lee and T.-L. Choi, *J. Am. Chem. Soc.*, 2013, **135**, 17695.
- 12 (a) T. Ogoshi, Y. Nishida, T. Yamagishi and Y. Nakamoto, *Macromolecules*, 2010, **43**, 7068; (b) Z. Zhang, B. Xia, C. Han, Y. Yu and F. Huang, *Org. Lett.*, 2010, **12**, 2385; (c) C. Li, L. Zhao, J. Li, X. Ding, S. Chen, Q. Zhang, Y. Yu and X. Jia, *Chem. Commun.*, 2010, **46**, 9016; (d) W. Si, X.-B. Hu, X.-H. Liu, R. Fan, Z. Chen, L. Weng and J.-L. Hou, *Tetrahedron Lett.*, 2011, **52**, 2484; (e) Y. Yao, M. Xue, J. Chen, M. Zhang and F. Huang, *J. Am. Chem. Soc.*, 2012, **134**, 15712; (f) Z. Zhang, C. Han, G. Yu and F. Huang, *Chem. Sci.*, 2012, **3**, 3026; (g) H. Deng, X. Shu, X. Hu, J. Li, X. Jia and C. Li, *Tetrahedron Lett.*, 2012, **53**, 4609; (h) Y. Yao, M. Xue, Z. Zhang, M. Zhang, Y. Wang and F. Huang, *Chem. Sci.*, 2013, **4**, 3667; (i) H. Li, D.-X. Chen, Y.-L. Sun, Y. Zheng, L.-L. Tan, P. S. Weiss and Y.-W. Yang, *J. Am. Chem. Soc.*, 2013, **135**, 1570; (j) J.-F. Xu, Y.-Z. Chen, L.-Z. Wu, C.-H. Tung and Q.-Z. Yang, *Org. Lett.*, 2013, **15**, 6148; (k) S. Sun, X.-Y. Hu, D. Chen, J. Shi, Y. Dong, C. Lin, Y. Pan and L. Wang, *Polym. Chem.*, 2013, **4**, 2224–2229; (l) S. Dong, J. Yuan and F. Huang, *Chem. Sci.*, 2014, **5**, 247; (m) D.-D. Zheng, D.-Y. Fu, Y. Wu, Y.-L. Sun, L.-L. Tan, T. Zhou, S.-Q. Ma, X. Zha and Y.-W. Yang, *Chem. Commun.*, 2014, **50**, 3201; (n) Y. Yao, X. Chi, Y. Zhou and F. Huang, *Chem. Sci.*, 2014, DOI: 10.1039/C4SC00585F; (o) Z.-Y. Li, Y. Zhang, C.-W. Zhang, L.-J. Chen, C. Wang, H. Tan, Y. Xu, L. Li and H.-B. Yang, *J. Am. Chem. Soc.*, 2014, DOI: 10.1021/ja413047r.
- 13 (a) D. Cao, Y. Kou, J. Liang, Z. Chen, L. Wang and H. Meier, *Angew. Chem. Int. Ed.*, 2009, **48**, 9721; (b) C. Han, F. Ma, Z. Zhang, B. Xia, Y. Yu and F. Huang, *Org. Lett.*, 2010, **12**, 4360; (c) M. Xue, Y. Yang, X. Chi, Z. Zhang and F. Huang, *Acc. Chem. Res.*, 2012, **45**, 1294; (d) Y. Ma, X. Chi, X. Yan, J. Liu, Y. Yao, W. Chen, F. Huang and J.-L. Hou, *Org. Lett.*, 2012, **14**, 1532; (e) P. J. Cragg and K. Sharma, *Chem. Soc. Rev.*, 2012, **41**, 597; (f) W. Chen, Y. Zhang, J. Li, X. Lou, Y. Yu, X. Jia and C. Li, *Chem. Commun.*, 2013, **49**, 7956; (g) I. Nierengarten, S. Guerra, M. Holler, L. Karmazin-Brelot, J. Barberá, R. Deschenaux and J.-F. Nierengarten, *Eur. J. Org. Chem.*, 2013, 3675. (h) C. Han, L. Gao, G. Yu, Z. Zhang, S. Dong and F. Huang, *Eur. J. Org. Chem.*, 2013, 2529; (i) X. Chi, M. Xue, Y. Ma, X. Yan and F. Huang, *Chem. Commun.*, 2013, **49**, 8175.
- 14 (a) S. Wang, Y. Liu, H. Liu, G. Yu, Y. Xu, X. Zhan, F. Xi and D. Zhu, *J. Phys. Chem. B*, 2002, **106**, 10618; (b) F. Huang, D. S. Nagvekar, C. Slebodnick and H. W. Gibson, *J. Am. Chem. Soc.*, 2005, **127**, 484; (c) W.-H. Huang, P. Y. Zavalij and L. Isaacs, *Angew. Chem. Int. Ed.*, 2007, **46**, 7425; (d) Z. Niu and H. W. Gibson, *Chem. Rev.*, 2009, **109**, 6024; (e) W. Jiang, A. Schäfer, P. C. Mohr and C. A. Schalley, *J. Am. Chem. Soc.*, 2010, **132**, 2309; (f) Z. Niu, F. Huang and H. W. Gibson, *J. Am. Chem. Soc.*, 2011, **133**, 2836; (g) L. Chen, Y.-K. Tian, Y. Ding, Y.-J. Tian and F. Wang, *Macromolecules*, 2012, **45**, 8412–8419; (h) K. Zhu, V. N. Vukotic and S. J. Loeb, *Angew. Chem. Int. Ed.*, 2012, **51**, 2168; (i) D.-S. Guo and Y. Liu, *Chem. Soc. Rev.* 2012, **41**, 5907; (j) Z. Qi, P. M. Molina, W. Jiang, Q. Wang, K. Nowosinski, A. Schulz, M. Gradzielski and C. A. Schalley, *Chem. Sci.*, 2012, **3**, 2073; (k) B. Vinciguerra, L. Cao, J. R. Cannon, P. Y. Zavalij, C. Fenselau and L. Isaacs, *J. Am. Chem. Soc.*, 2012, **134**, 13133; (l) S.-L. Li, T. Xiao, C. Lin and L. Wang, *Chem. Soc. Rev.*, 2012, **41**, 5950; (m) F. Wang, M. Gillissen, P. J. M. Stals, A. R. A. Palmans and E. W. Meijer, *Chem. Eur. J.*, 2012, **18**, 11761–11770; (n) S. Li, J. Huang, F. Zhou, T. R. Cook, X. Yan, Y. Ye, B. Zhu, B. Zheng and P. J. Stang, *J. Am. Chem. Soc.*, 2014, **136**, 5908; (o) S. Li, G.-H. Peng, W. Lin, Z.-B. Sun, M. Zhou, B. Zhu, Y. Ye and J. Wu, *Polym. Chem.*, 2014, DOI: 10.1039/C4PY00409D.
- 15 (a) Z. Zhang, G. Yu, C. Han, J. Liu, X. Ding, Y. Yu and F. Huang, *Org. Lett.*, 2011, **13**, 4818; (b) N. L. Strutt, R. S. Forgan, J. M. Spruell, Y. Y. Bottros and J. F. Stoddart, *J. Am. Chem. Soc.*, 2011, **133**, 5668; (c) Z. Zhang, Y. Luo, J. Chen, S. Dong, Y. Yu, Z. Ma and F. Huang, *Angew. Chem. Int. Ed.*, 2011, **50**, 1397; (d) W. Si, L. Chen, X.-B. Hu, G. Tang, Z. Chen, J.-L. Hou and Z.-T. Li, *Angew. Chem. Int. Ed.*, 2011, **50**, 12564; (e) L. Liu, L. Wang, C. Liu, Z. Fu, H. Meier and D. Cao, *J. Org. Chem.*, 2012, **77**, 9413; (f) G. Yu, Z. Zhang, C. Han, M. Xue, Q. Zhou and F. Huang, *Chem. Commun.*, 2012, **48**, 2958; (g) Y. Guan, M. Ni, X. Hu, T. Xiao, S. Xiong, C. Lin and L. Wang, *Chem. Commun.*, 2012, **48**, 8532; (h) X. Wang, K. Han, J. Li, X. Jia and C. Li, *Polym. Chem.*, 2013, **4**, 3998; (i) X.-Y. Hu, X. Wu, S. Wang, D. Chen, W. Xia, C. Lin, Y. Pan and L. Wang, *Polym. Chem.*, 2013, **4**, 4292. (j) L. Chen, W. Si, L. Zhang, G. Tang, Z.-T. Li and J.-L. Hou, *J. Am. Chem. Soc.*, 2013, **135**, 2152. (k) Q. Duan, Y. Cao, Y. Li, X. Hu, T. Xiao, C. Lin, Y. Pan and L. Wang, *J. Am. Chem. Soc.*, 2013, **135**, 10542; (l) G. Yu, Y. Ma, C. Han,

Journal Name

- Y. Yao, G. Tang, Z. Mao, C. Gao and F. Huang, *J. Am. Chem. Soc.*, 2013, **135**, 10310 (m) Z. Zhang, Q. Zhao, J. Yuan, M. Antonietti and F. Huang, *Chem. Commun.*, 2014, **50**, 2595.
- 16 (a) S. Fukushima, K. Miyata, N. Nishiyama, N. Kanayama, Y. Yamasaki and K. Kataoka, *J. Am. Chem. Soc.*, 2005, **127**, 2810; (b) C. Wang, Y. Kang, K. Liu, Z. Li, Z. Wang and X. Zhang, *Polym. Chem.*, 2012, **3**, 3056.